Journal of
Ceramic Science
and Technology

J. Ceram. Sci. Tech., **08** [01] 53-58 (2017)
DOI: 10.4416/JCST2016-00087
available online at: http://www.ceramic-science.com

Residual Strength Evolution of 2D C/C-SiC Composites Subjected to Tensile Fatigue Stresses

B.-G. Zhang[1], Y. Li[1, 2], P. Xiao[*1], W. Zhou[1, 3], H. Luo[1], Z. Li[*1]

[1]State Key Laboratory of Powder Metallurgy, Central South University, Changsha, 410083, PR China
[2]Ceramic Materials Engineering, University of Bayreuth, Bayreuth, 95447, Germany
[3]College of Metallurgical Engineering, Hunan University of Technology, Zhuzhou, 412008, PR China
received October 20, 2016; received in revised form November 7, 2016; accepted November 15, 2016

Abstract

An experimental investigation was performed to study the residual tensile strength (RTS) of liquid silicon infiltration (LSI)-based plain-weave reinforced C_f/C-SiC composites (2D C/C-SiC) after different loading cycles. The specimens were previously subjected to the cyclic stress of 57 MPa for the preselected numbers of cycles (10^2, 10^4 and 10^6, respectively) before the final quasi-static tensile test. The microstructures, fractured surfaces and coefficient of thermal expansion (CTE) after the quasi-static tensile test were characterized by means of Optical Microscopy (OM), Scanning Electron Microscopy (SEM) and a classical mechanical push-rod dilatometer, respectively. The results showed that the RTS of the specimens after the preselected fatigue cycles numbers of 10^2, 10^4 and 10^6 increase to 90.9, 94.1 and 84.5 MPa, respectively, which are somewhat higher than that of virgin samples (79.7 MPa). Additionally, the tensile stress-strain curves of the post-fatigue specimens present cycle-independence within the region of linear response. Finally, the CTE in the range of 200 – 1000 °C gradually decreased with the increasing cycles owing to higher damage induced by fatigue stress along the loading direction.

Keywords: C/C-SiC, fatigue, cracking, residual strength

I. Introduction

Liquid silicon infiltration (LSI) has been widely applied to fabricate high-performance C/C-SiC composites with favorable efficiency and relatively low cost[1]. The plain-weave carbon fabric, as a typical architecture of fibers, is widely applied as reinforcement for C/C-SiC composites (2D C/C-SiC) with high specific strength/modulus and favorable fracture toughness[2]. So far these 2D C/C-SiC composites have been used in high-performance braking systems and space structures, etc[3]. Generally, the mechanical properties of C/C-SiC composites under inevitable fluctuant loads should be considered. Note that the cyclic stress could result in mechanical degradation and catastrophic failure[4, 5]. Therefore, the investigation of the mechanical evolution of C/C-SiC composites under complex combinations of loads in the long term is of importance. Despite the fact that fatigue behavior and fatigue damage mechanisms, including cracking and interfacial debonding, etc., for ceramic matrix composites (CMC) have been studied extensively for decades[5–7], it is still necessary to understand more about the fatigue behavior of these materials, especially the LSI-based C/C-SiC composites. Hence, the current work deals with the effect of fatigue damage on the residual tensile strength (RTS) of 2D C/C-SiC composites. The RTS of the specimens loaded after 10^2, 10^4 and 10^6 cycles was investigated experimentally, and the microstructures, the fractured surfaces and CTE of the specimens were analyzed.

II. Materials and Experimental Procedures

The flow diagram for the manufacture process of 2D C/C-SiC composites is shown in Fig. 1. Four main procedures including impregnation, warm-press, pyrolysis and LSI were involved in this work. Firstly, the HTA plain-weave fabric (Toho-Tenax HTA 460 – 5) and a phenolic resin with a carbon yield of about 50 % were used as reinforcement material and carbon precursor, respectively. The carbon-fiber-reinforced plastics (CFRP) for the C/C-SiC composites were fabricated with laminated 2D plain-weave carbon fabrics. Note that the fabrics were firstly pre-impregnated with a phenolic resin solution in isopropanol and then dried at 20 °C for 48 h. After the fabric layers had been stacked over some additional phenolic resin powder, the warm-press process was performed to fabricate the CFRP with a fiber volume fraction of approximately 50 %. Afterwards, pyrolysis was performed in flowing nitrogen atmosphere up to 1000 °C. The minimum heating rate of the pyrolysis was set to 0.5 K/min. Finally, silicon infiltration was conducted at > 1420 °C with 1 h dwell time under vacuum conditions.

The open porosity and bulk density of the as-prepared composites were measured with the Archimedes method, in compliance with DIN EN 1389. Addition-

* Corresponding author: xiaopengcsu@csu.edu.cn, lizhuan@csu.edu.cn

ally, the quasi-static tensile tests were conducted on a Zwick/Roell test machine (Z1485, Makro, 250 kN) with the dog-bone-shaped specimens shown in Fig. 2, in line with DIN EN 658 – 1.

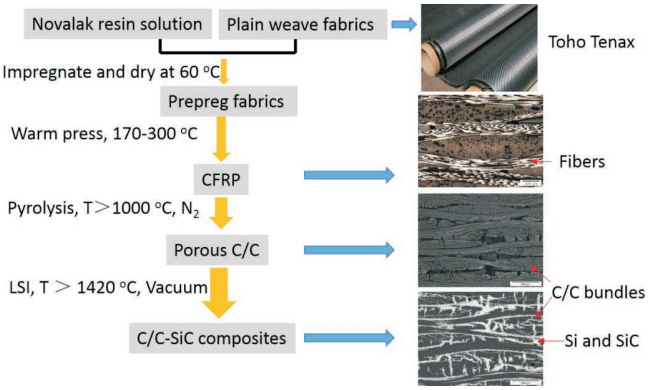

Fig. 1: Flow diagram for the preparation of 2D C/C-SiC composites.

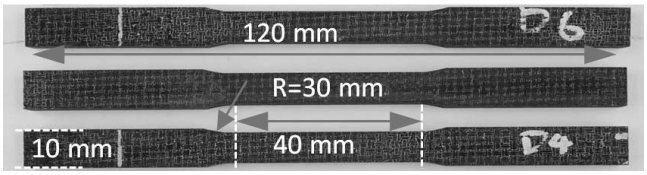

Fig. 2: The specimens for the static tensile/fatigue test.

The loading rate for the quasi-static tensile test was set to 1 mm/min. Moreover, the tensile fatigue test was conducted on a servo hydraulic testing machine (IST Hydro pulse MHF), following ASTM C1360. All these tests with a preselected number of cycles (10^2, 10^4 and 10^6, respectively) were performed in a strain-control mode with the following parameters: sinusoidal wave, frequency of 10 Hz, maximum fatigue stress of 57 MPa and stress ratio of 0.1. Thermal expansion measurements for the virgin and post-fatigue specimens were performed in a classical mechanical push-rod dilatometer (NETZSCH DIL 402 E) with a temperature range of 200 – 1000 °C and heating rate of 10 °C min^{-1} in the nitrogen atmosphere. The linear CTE was measured as defined by Equation (1):

$$\alpha = \frac{\varepsilon}{\Delta T} = \frac{\Delta 1}{1_0 \Delta T} \quad (1)$$

where α is the coefficient of thermal expansion, ΔT is the temperature interval, 1_0 is the length of the virgin sample before test, and $\Delta 1$ is the relative change in length.

Finally, the microstructures and fractured surfaces of the specimens were characterized with an optical microscope (Axiotech HAL100, Zeiss), and a scanning electron microscope (SEM, FEI Nova Nano SEM-230), respectively.

III. Results and Discussion

The basic properties of the as-prepared C/C-SiC composites before the fatigue test are summarized in Table 1.

As shown in Table 1, the porosity and density of the as-prepared C/C-SiC composites were approximately 2.8 % and 1.95 gcm^{-3}, respectively. Moreover, the tensile strength and tensile modulus for the virgin specimens under quasi-tensile test were 79.7 MPa and 45.1 GPa, respectively.

(1) Fatigue behavior of 2D C/C-SiC composites

Fig. 3 shows the tensile fatigue life S-N curve of C/C-SiC composites at room temperature. Clearly, the as-prepared C/C-SiC composites show high resistance to fatigue stress. The fatigue limit (1 million cycles) for the C/C-SiC in this work is around 57 MPa. Therefore, the maximum fatigue stress of 57 MPa with preselected cycles was applied to the specimens in order to avoid fracture before the final quasi-static tensile test.

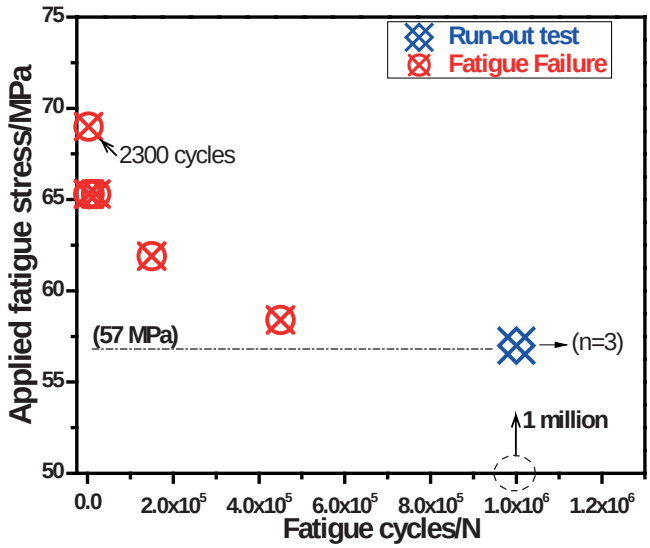

Fig. 3: Tensile fatigue life S-N curve of C/C-SiC composites.

Fig. 4 shows the evolution of the dynamic modulus (DM) and permanent strain (PS) during fatigue loading. It is well known that PS is related to fatigue damage [5]. As plotted in the Fig. 4, the slope of the PS versus fatigue cycles is reduced with the increment of fatigue cycles, indicating that the growth rate of PS gradually decreases with the increased cycles. Moreover, the decreased DM and the increased PS in the beginning are closely associated with the rapid initiation and growth of pre-existing matrix cracks, fiber breakage and interfacial debonding [9, 10]. Additionally, it is recommended that the initial PS within

Table 1: General properties of the C/C-SiC composites.

Bulk density/gcm^{-3}	Open porosity/%	Quasi- static tensile strength/MPa	Failure strain/%	Tensile modulus /GPa	Number of tested sample
1.95±0.03	2.8±0.3	79.7 ±7	0.21±0.05	45.1±4.5	N=7

hundreds of cycles primarily results from the poor closure of extended cracks in the transverse bundles[11, 12]. Afterwards, the progressive change of PS reveals that both the formation and the propagation of cracks (near crack saturation) barely take place. As the fatigue cycling progresses, the DM is seemingly constant owing to the roughly saturated fatigue damage. Based on the different growth rates of PS during the fatigue loading, hereinafter three number of fatigue cycles (10^2, 10^4, 10^6) are identified to study the influence of fatigue damage on the RTS. Therefore, many post-fatigue specimens with the preselected loading cycles were tested for their RTS.

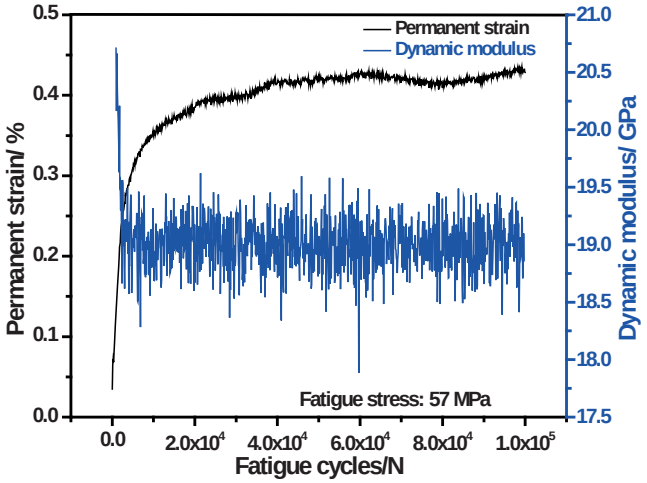

Fig. 4: Permanent strain and dynamic modulus versus fatigue cycles[8].

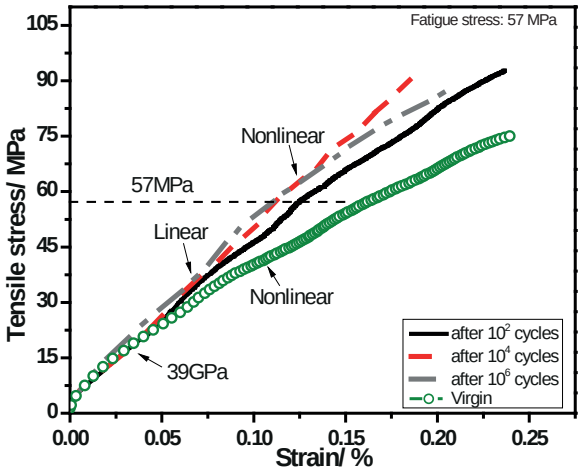

Fig. 5: Typical tensile stress-strain curves for the virgin and post-fatigue specimens.

Fig. 5 presents the representative tensile stress-strain (S-S) curves for virgin and post-fatigue C/C-SiC specimens. The S-S curve of the virgin specimen substantially shows a non-linear response which is derived from matrix cracking and fiber breakage. However, the stress-strain curves of the post-fatigue specimens show roughly linear behavior, when the tensile stress during the quasi-static test is lower than the maximum fatigue stress (57 MPa). Note that the linear behavior for the post-fatigue specimens is independent of the increasing fatigue cycles, indicating that the cracks are already well propagated during the initial fatigue cycles. Only if the applied tensile stress is higher than 57 MPa, new damage, for example, cracks and interfacial degradation, are detectable, which is in accordance with previous experimental results[13, 14]. The nonlinear behavior of the post-fatigue samples occurs with the beginning of the fiber rupture and cracking, similar to the virgin sample. Furthermore, the results of the quasi-static tensile tests for the C/C-SiC samples after 10^2, 10^4 and 10^6 cycles are summarized in Fig. 6.

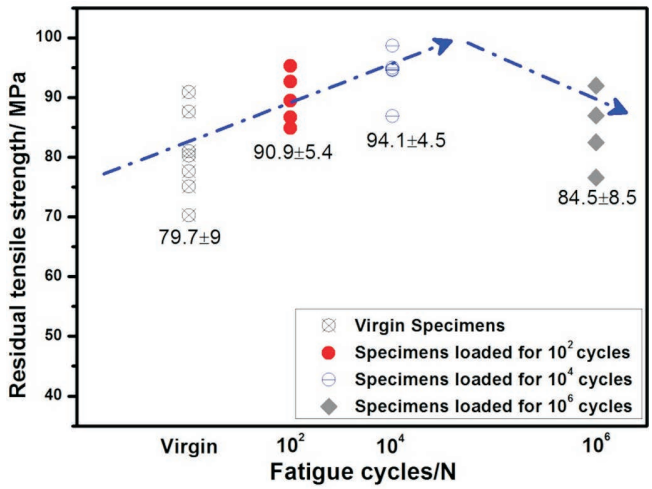

Fig. 6: Diagram of RTS for virgin and post-fatigue C/C-SiC.

Fig. 6 shows the distribution of the RTS value for the virgin and post-fatigue specimens.

It is clear that the fatigue-induced enhancement for RTS can be observed beyond 10^2 cycles. The mean values of RTS for the post-fatigue specimens after 10^2, 10^4 and 10^6 loading cycles are approximately 90.9, 94.1 and 84.5 MPa, respectively, which are somewhat higher than that of virgin specimens (79.7 MPa). Additionally, it is generally known that the strength enhancement or the strength degradation induced by fatigue damage is dependent on the length of fatigue period[14, 15]. Excessive fatigue loading for a very long period, for example, exceeding 10^6 cycles, will undoubtedly be detrimental to the strength. As shown in Fig. 6, the initially increased fatigue damage could lead to a more prominent effect on enhancement than degradation in RTS. However, these effects will reverse when the specimens are subjected to fatigue loading for a longer duration. It is shown that the RTS after 10^4 cycles is higher than those of 10^2 and 10^6 cycles. Hence, the most pronounced influence of the fatigue damage on the RTS is seemingly approached after 10^4 cycles in the current work. Based on the current experimental results, it could be deduced that the RTS of C/C-SiC will further decrease as the fatigue cycle number exceeds 10^6, until occurrence of tensile fracture.

(2) Microstructure of C/C-SiC before and after fatigue

Fig. 7 displays the typical cross-sectional microstructures for the virgin C/C-SiC and post-fatigue C/C-SiC after 10^6 cycles. In order to characterize the fatigue-induced damage, all the micro-cracks in Fig. 7(a) and Fig. 7(c) are marked with red arrows. The cracks shown in Fig. 7(a) are derived from the mismatch of the CTE between the fibers and matrix during the cooling procedure from the

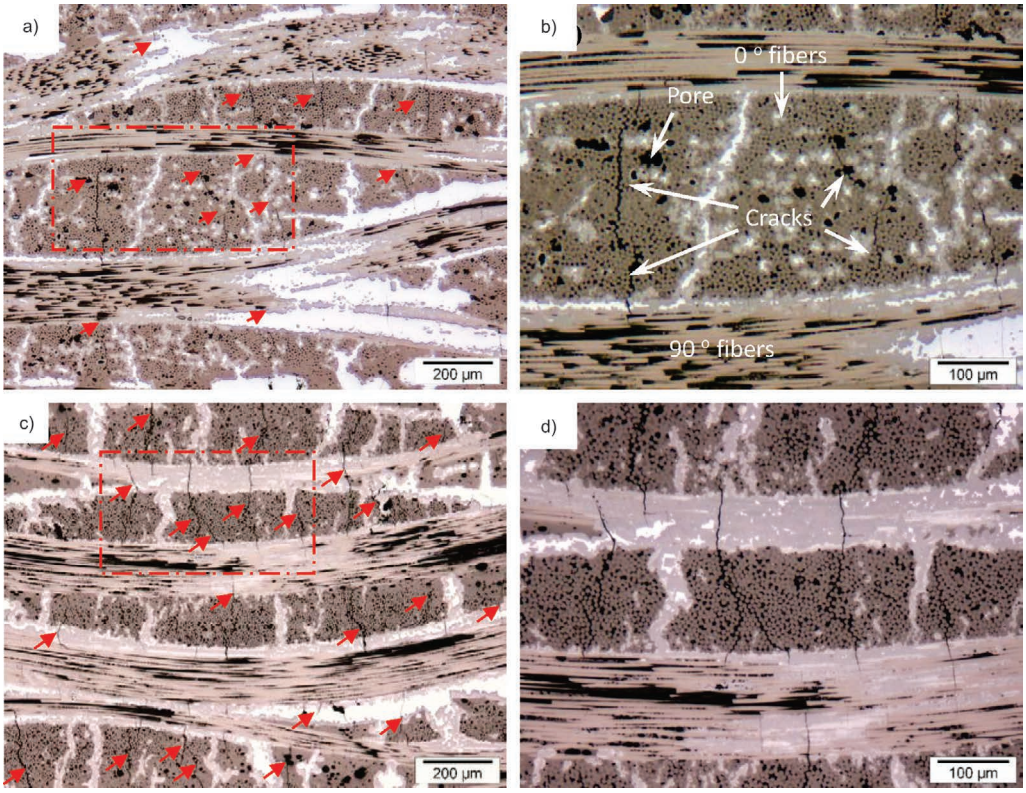

Fig. 7: Typical microstructure of C/C-SiC under OM; (a) Virgin specimen; (b) Magnification of the highlighted area in Fig. 7(a); (c) Post-fatigue specimen after 10^6 cycles; (d) Magnification of highlighted area in Fig. 7(c); Cracks are marked by the red arrows; the loading direction is parallel to the 90° fibers.

LSI process temperature to room temperature in which the 0° fibers will suffer tensile thermal residual stress whereas the compressive stress will be generated in the 90° fibers. Therefore, most of these cracks distribute in the 0° fiber bundles with the orientation vertical to the 90° fibers. Additionally, some short cracks (see Fig. 7(b)) could be observed within the 0° fibers segment and they probably extend towards to the 90° orientated fibers when fatigue stress is applied.

Fig. 7(c) and Fig. 7(d) display the microstructures of the post-fatigue specimen after 10^6 cycles. The increased number of long cracks, which are bridging the adjacent 90° orientated fiber bundles, can be observed in Fig. 7(d). Note that some fully extended cracks after cyclic loading are stopped in the front of 90° bundles and these cracks under fatigue loading will propagate along the 90° fiber bundles (see Fig. 8).

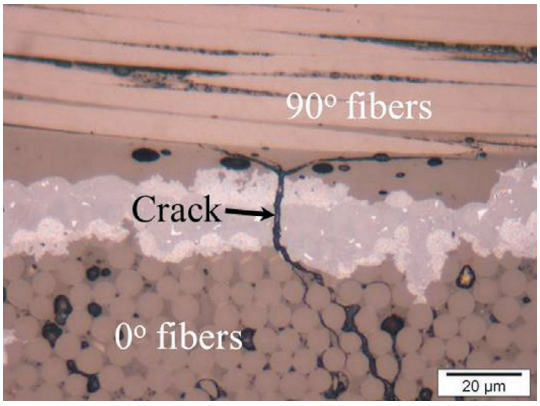

Fig. 8: Crack propagation along the 90° fibers.

In order to make a comparison of the microstructures before and after fatigue loading, the density of the micro-cracks (see Table 2) was calculated using the optical microscope. The crack numbers of each sample in twenty-one different regions, each with an area of approximately 1.55 mm^2, which is equal to the area of Fig. 7(a), were summed up to calculate the mean value of the crack density. As shown in Table 2, crack density within the identical area seemingly increases with the cumulative cycles.

Table 2: Statistics data of crack density in the C/C-SiC composites.

C/C-SiC Sample	Fatigue stress and cycles	Number of micro-cracks (mean value) per 1.55 mm^2	Number of observed region
Virgin	No	10.5 (4.5)	N=21
Post- fatigue	57 MPa, 10^2	11.7 (2.3)	N=21
Post- fatigue	57 MPa, 10^4	15.1 (3.8)	N=21
Post-fatigue	57 MPa, 10^6	18.1 (2.5)	N=21

Standard deviations are given in parentheses.

The CTE in the direction of 90° orientated fibers for the virgin and post-fatigue specimens is listed in Table 3. Compared to the virgin specimens, the CTE for the post-fatigue specimens after one million cycles was apparently reduced. Generally, the CTE along the 90° fiber orientation

relates to the matrix and the 0° fiber segment in this work because the axial thermal expansion of the fiber is negligible[16]. Therefore, the lower CTE in the post-fatigue specimens indicates more defects, especially cracks, induced by fatigue loading within the 0° fibers bundles.

Table 3: CTE of the virgin and post-fatigue C/C-SiC specimens along the 90° fiber orientation.

C/C-SiC Sample	Fatigue stress and cycles	Average CTE/$10^{-6}K^{-1}$ (mean value from 200 °C-1000 °C)	Number of tested specimens
Virgin	No	3.09	N=2
Post-fatigue	57 MPa, 10^6	0.82	N=2

Based on the statistics of crack density and CTE measurement, it could be concluded that one instance of major damage caused by fatigue stress is the variation of cracks in the matrix. Note that the multiplication and propagation of cracks in the 0° fiber bundles can effectively relieve the thermal residual stress in the composites, which enables more fiber bundles to carry the applied load uniformly and simultaneously, resulting in strength enhancement[17].

Fig. 9 displays the typical fractured surfaces for virgin and post-fatigue specimens after the quasi-static tensile tests. As shown in Fig. 9(a), the fiber bundles in the fractured surface of virgin specimen are compact. Moreover, only few single fiber pull-outs and limited interfacial detaching between fiber/matrix can be observed. The fractured surfaces for the post-fatigue specimens after 10^2, 10^4 and 10^6 cycles are show in Fig. 9 (b-d), respectively.

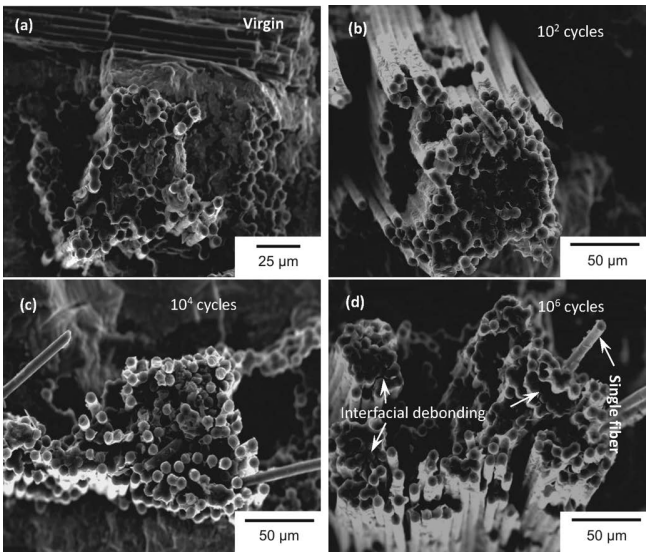

Fig. 9: The fractured surfaces of C/C-SiC composites (SEM images, topography contrast), (a) Virgin sample; (b) Post-fatigue specimen after 10^2 cycles[8]; (c) Post-fatigue specimen after 10^4 cycles[8]; and (d) Post-fatigue specimen after 10^6 cycles.

Compared to Fig. 9(c-d), the fractured surface of the fatigue specimens after 10^2 cycles is very similar to that of the virgin specimens, displaying few instances of interfacial debonding. The fatigue damage after 10^2 fatigue cycles are mainly in the form of the crack propagation in matrix. However, more single fibers and interfacial debonding can be observed within the pulled-out fiber bundle segments in the fractured surfaces for the post-fatigue specimens, as shown in Fig. 9(c) and Fig. 9(d). It is well-established fact that more pull-out of single fibers indicates further interfacial degradation between the fiber and matrix.

Fig. 10 displays the representative interfaces between carbon fiber and matrix in virgin and post-fatigue specimens. As shown in Fig. 10(a), the bonding between fiber/matrix in the virgin sample is intact. However, the interfacial debonding between the fiber and matrix as shown in Fig. 10(b) was induced by fatigue stress.

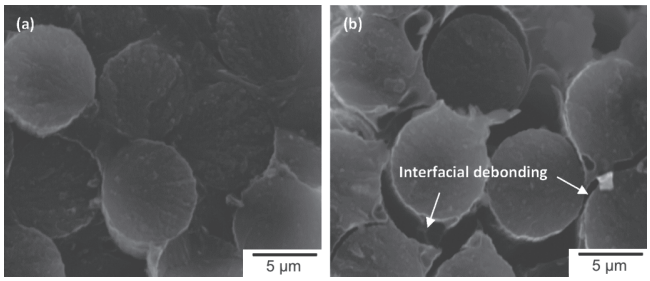

Fig. 10: SEM image of the interface between carbon fiber and matrix, (a) Intact interface in the virgin sample; (b) Interfacial debonding in the post-fatigue sample.

As is well known that interfacial debonding exerts profound influence on the RTS as the loading cycle proceeds. On the one hand, the interfacial debonding could decrease the stress concentration in the crack tip and enable crack deflection more probably than the penetration of a crack directly into the fibers. As a result, the fatigue-loaded specimens are enhanced in short-term loading. On the other hand, interfacial wear, which is derived from the interfacial debonding, will lead to reduced interfacial sliding resistance and introduce new flaws into the fibers in the long term. The damaged fibers are definitely detrimental to the RTS. Hence, the specimens after 10^6 cycles show a decreased RTS in comparison to others owing to the interfacial wear. In other words, the interaction of interfacial degradation and matrix cracking lead to increased fatigue damage and higher permanent strain with the increasing cycles, which makes the RTS first rise in the short term (less than 10^4 cycles) then fall in the long term (more than 10^6 cycles).

IV. Conclusions

The residual tensile strength (RTS) of C/C-SiC composites subjected to a fatigue stress of 57 MPa for three preselected loading cycles (10^2, 10^4 and 10^6) was investigated. The microstructures, fractured surfaces and coefficient of thermal expansion of the virgin and post-fatigue specimens were characterized to study the fatigue-induced damage. Based on the performed investigations, the following conclusions are drawn:

(1) The crack multiplication and propagation caused by fatigue stress results in a decreased CTE. Compared to the virgin specimens (3.09), the CTE in 90° fiber orientation after 10^6 cycles is approximately 0.82.

(2) The linear behavior in the stress-strain curve during the quasi-static tensile test is independent of the number of the previously loaded cycles.
(3) The interaction of the matrix cracking and interfacial degradation in C/C-SiC composites induced by fatigue stress could lead to strength enhancement, even after 10^6 cycles. However, the maximum RTS of 94.1 MPa was obtained after 10^4 cycles, which is somewhat higher than that of the virgin samples (79.7 MPa).
(4) The interfacial wear derived from the interfacial degradation results in gradually decreased RTS in the long term.

Acknowledgements

The project was supported by the National Key Research and Development Program of China under Grant No. 2016YFB0301403 and the National Science Foundation of China under Grant No. 51575536. Additionally, the authors would like to express their heartfelt gratitude to Prof. Walter Krenkel, Dr. Nico Langhof and Mr. Florian Reichert from Ceramic Materials Engineering, University of Bayreuth, for their contributions in the raw materials and academic discussions, to Mr. A. Brückner and Mr. A. Mainz from the Department of Polymer Engineering, University of Bayreuth for their kind assistance in mechanical tests. All experimental tests in this study were conducted at Ceramic Materials Engineering, University of Bayreuth.

References

1 Krenkel, W.: Carbon fiber reinforced CMC for high-performance structures, *Int. J. Appl. Ceram. Tec.*, **1**, 188 – 200, (2004).
2 Krenkel, W., Renz, R.: in *Ceramic Matrix Composites*, Wiley-VCH Verlag GmbH & Co. KGaA, pp. 385 – 407, (2008).
3 Krenkel, W., Berndt, F.: C/C-SiC composites for space applications and advanced friction systems. *Mat. Sci. Eng. A*, **412**, 177 – 181, (2005).
4 Evans, A.G., Zok, F.W., McMeeking, R.M.: Fatigue of ceramic matrix composites. *Acta. Mater.*, **43**, 859 – 875, (1995).
5 Reynaud, P.: Cyclic fatigue of ceramic-matrix composites at ambient and elevated temperatures. *Compos. Sci. Techol.*, **56**, 809 – 814, (1996).
6 Marshall, D. B., Evans, A.G.: Failure mechanisms in ceramic-fiber/ceramic-matrix composites. *J. Am. Ceram. Soc.*, **68**, 225 – 231, (1985).
7 Dassios, K.G., Aggelis, D.G., Kordatos, E.Z., Matikas, T.E.: Cyclic loading of a SiC-fiber reinforced ceramic matrix composite reveals damage mechanisms and thermal residual stress state, *Compos. Part. A-Appl. S.*, **44**, 105 – 113, (2013).
8 Li, Y., Xiao, P., Li, Z., Zhou, W.: Strength evolution of cyclic loaded LSI-based C/C-SiC composites. *Ceram. Int.*, **42**, 14505 – 14510, (2016).
9 Zhang, Y., Cheng, L., Zhang, L., Luan, X.: Comparative analysis of low-cycle fatigue behavior of 2D-C_f-P_yC/SiC composites in different environments, *Int. J. Appl. Ceram. Tec.*, **12**, 491 – 499, (2015).
10 Gumula, T., Rudawski, A., Michalowski, J., Blazewicz, S.: Fatigue behavior and oxidation resistance of carbon/ceramic composites reinforced with continuous carbon fibers, *Ceram. Int.*, **41**, 7381 – 7386, (2015).
11 Reynaud, P., Dalmaz, A., Tallaron, C., Rouby, D.: Apparent stiffening of ceramic-matrix composites induced by cyclic fatigue, *J. Eur. Ceram.Soc.*, **18**, 1827 – 1833, (1998).
12 Fantozzi, G., Reynaud, P.: Mechanical hysteresis in ceramic matrix composites. *Mat. Sci. Eng. A*, **521 – 522**, 18 – 23, (2009).
13 Mei, H., Cheng, L.: Stress-dependence and time-dependence of the post-fatigue tensile behavior of carbon fiber reinforced SiC matrix composites. *Compos. Sci. Techol.*, **71**, 1404 – 1409, (2011).
14 Li, Y., Xiao, P., Luo, H., Almeida, R.S.M.: Fatigue behavior and residual strength evolution of 2.5D C/C-SiC composites. *J. Eur. Ceram.Soc.*, **36**, 3977 – 3985, (2016).
15 Fang, G., Gao, X., Zhang, S., Xue, J.: A residual strength model for the fatigue strengthening behavior of 2D needled CMCs. *Int. J. Fatigue.*, **80**, 298 – 305, (2015).
16 Bansal, N.P., Lamon, J.: *Ceramic Matrix Composites: Materials, Modeling and Technology,* John Wiley & Sons, (2014).
17 Mizuno, M., Zhu, S., Nagano, Y., Sakaida, Y.: Cyclic-fatigue behavior of SiC/SiC composites at room and high temperatures. *J. Am. Ceram. Soc.*, **79**, 3065 – 3077, (1996).